Magnetic Resonance in Medicine 54:1040–1045 (2005)

Convergence Behavior of Iterative SENSE Reconstruction with Non-Cartesian Trajectories

Peng Qu,[1] Kai Zhong,[2] Bida Zhang,[2,3] Jianmin Wang,[3] and Gary X. Shen[1]*

In non-Cartesian SENSE reconstruction based on the conjugate gradient (CG) iteration method, the iteration very often exhibits a "semi-convergence" behavior, which can be characterized as initial convergence toward the exact solution and later divergence. This phenomenon causes difficulties in automatic implementation of this reconstruction strategy. In this study, the convergence behavior of the iterative SENSE reconstruction is analyzed based on the mathematical principle of the CG method. It is revealed that the semi-convergence behavior is caused by the ill-conditioning of the underlying generalized encoding matrix (GEM) and the intrinsic regularization effect of CG iteration. From the perspective of regularization, each iteration vector is a regularized solution and the number of iterations plays the role of the regularization parameter. Therefore, the iteration count controls the compromise between the SNR and the residual aliasing artifact. Based on this theory, suggestions with respect to the stopping rule for well-behaved reconstructions are provided. Simulated radial imaging and in vivo spiral imaging are performed to demonstrate the theoretical analysis on the semi-convergence phenomenon and the stopping criterion. The dependence of convergence behavior on the undersampling rate and the noise level in samples is also qualitatively investigated. Magn Reson Med 54:1040–1045, 2005.

Key words: parallel imaging; SENSE; non-Cartesian trajectories; conjugate-gradient; regularization; image reconstruction

Parallel imaging techniques have shown potential to revolutionize the field of fast MRI in recent years (1–11). By using sensitivity information from an RF coil array to perform some of the spatial encoding that is traditionally accomplished by magnetic field gradient, parallel imaging allows reduction of phase encoding steps and consequently decreases the scan time. Several practical parallel imaging reconstruction strategies have been proposed, including the *k*-space based simultaneous acquisition of spatial harmonics (SMASH) (2–5), the generalized auto-calibrating partially parallel acquisitions (GRAPPA) (6), and the image-domain based sensitivity encoding (SENSE) approach (7).

In general, the essence of parallel imaging reconstruction is to solve a linear system of equations (LSE) representing the encoding scheme, or more specifically, to inverse the generalized encoding matrix (GEM) produced by magnetic gradient modulation and coil sensitivity modulation (8). For image acquisitions of appreciable matrix size, the dimension of GEM is rather large, and straightforward inversion is numerically prohibitive. For the case of sampling along a regular Cartesian *k*-space grid, a Fourier transform may be separated out from the inversion process as a distinct step, and the GEM then attains a block diagonal structure and its processing can be significantly simplified. Specifically, in SENSE, each block corresponds to a set of aliased pixels, and the inversion becomes a block-by-block (pixel-by-pixel) inversion. However, for non-Cartesian *k*-space trajectories, such as spiral or radial schemes, such transformations of the GEM are no longer applicable because the *k*-space samples are not uniformly distributed and fast Fourier transform (FFT) cannot be applied in a straightforward manner. In these cases, the inversion of GEM is much more complicated and time-consuming. One efficient way is to perform reconstruction iteratively, as proposed by Pruessmann and Kannengießer (9–11). In this technique the large LSE is solved using the conjugate gradient (CG) iteration approach; and in executions of CG iteration loops, the most time-demanding matrix-vector multiplication procedure is efficiently implemented by combining gridding operations with FFT. In this fashion, the computational complexity of non-Cartesian SENSE reconstruction is reduced to the same order of magnitude as in conventional gridding reconstruction.

One of the important concerns in automatic implementation of this CG based iterative method is its convergence behavior. A preliminary investigation on convergence speed has been reported in Pruessmann's work (11). However, full understanding of the convergence behavior of iterative non-Cartesian SENSE reconstruction is still lacking so far. In particular, it is very often discovered in practical implementation that the reconstruction exhibits a "semi-convergence" characteristic, that is, the iteration vector initially approaches the desired exact solution and then, in later stages of the iteration, converge to some other undesired vector. Usually a small number of iterations are enough to obtain acceptable image quality for a well-behaved reconstruction. However, the number of iterations necessary to achieve satisfactory image quality differs significantly for different reconstructions. This makes an adaptive stopping criterion highly necessary for automatic implementation of this non-Cartesian SENSE technique.

In this study, the convergence behavior of the iterative non-Cartesian SENSE reconstruction strategy is analyzed based on the mathematic principle of the CG method. It is revealed that the semi-convergence behavior of reconstruction is caused by the ill-conditioning of the underlying LSE and the intrinsic regularization effect of CG itera-

[1]Department of Electrical and Electronic Engineering, the University of Hong Kong, Pokfulam, Hong Kong.

[2]Key Laboratory of Cognitive Science, The Graduate School and Institute of Biophysics, The Chinese Academy of Sciences, Beijing, China.

[3]Siemens Mindit Magnetic Resonance Ltd., Shenzhen, China.

Grant Sponsor: Hong Kong RGC Earmarked Research Grant; Grant Numbers: HKU 7045/01E and HKU 7170/03E.

*Correspondence to: Gary X. Shen, CYC 519, Department of Electrical and Electronic Engineering, The University of Hong Kong, Pokfulam, Hong Kong. E-mail: gxshen@eee.hku.hk

Received 25 March 2005; 3 June 2005; accepted 5 June 2005.

DOI 10.1002/mrm.20648

Published online 7 September 2005 in Wiley InterScience (www.interscience.wiley.com).

tion (12–14). From the perspective of regularization, each iteration vector is a regularized solution, and the number of iterations plays the role of the regularization parameter. As a consequence, the convergence behavior of non-Cartesian SENSE reconstruction is highly related to the SNR and artifact level. In particular, the stopping rule of the iteration is actually a compromise between the perturbation error, which controls the SNR, and the regularization error, which controls the residual aliasing artifacts. Based on this analysis, suggestions with respect to the stopping rule of the iteration are also provided. Simulated radial imaging and in vivo spiral imaging experiments are performed to investigate the convergence behavior of non-Cartesian SENSE reconstruction. The semi-convergence behavior is demonstrated, and its dependence on the undersampling rate and the noise level in samples is qualitatively studied.

THEORY

Review of CG-Based Iterative Non-Cartesian SENSE Reconstruction

The MR signal from a 2D slice detected by a given RF coil can be written as

$$S_\rho(k_x,k_y) = \int\int_{x,y} dxdyC_\rho(x,y) \quad [1]$$

where $M(x,y)$ represents the spin density in a 2-dimensional image plane labeled by Cartesian coordinates x and y, $C_\rho(x,y)$ represents the RF sensitivity for the ρ-th component coil in the array, and k_x, k_y are k-space coordinates.

Eq. [1] can be written in a matrix notation,

$$s = Em, \quad [2]$$

where s is the vector of signal samples, m is the vector of the unknown image, and E is the GEM composed of gradient encoding and coil sensitivity encoding.

In most cases, Eq. [2] is over-determined and usually solved in a least squares sense. For notational simplicity, we ignore the influence of the so-call sample noise correlation matrix since it can be diminished by reformulating with a decorrelation scheme (11); then the least squares estimate can be obtained by solving the normal equation form of Eq. [2], which reads:

$$(E^HE)m = E^Hs, \quad [3]$$

where the superscript H denotes the complex conjugate transpose.

According to Pruessmann (11), the CG iteration method is applied to Eq. [3]. Using the iteration scheme, the coefficient matrix is only accessed via matrix-vector multiplications, and a sequence of iteration vectors are produced that converge to the least squares solution. In each CG loop, the most time-consuming matrix-vector multiplication can be efficiently implemented using the gridding principle and FFT. Furthermore, for faster convergence, optional density and intensity correction can be introduced to the iterative reconstruction to precondition the ill-posed large LSE.

A variety of gridding algorithms can be employed in this technique. In this study, we chose the LS-nuFFT method proposed by Sha (15). The feasibility and efficiency of this gridding approach for non-Cartesian SENSE reconstruction has been demonstrated by Zhang (16).

Ill-Conditioning of the Generalized Encoding Matrix

In most cases, the GEM is undesirably ill-conditioned. This can be accounted for by the mixed Fourier-sensitivity encoding scheme underlying the GEM. For imaging with pure Fourier encoding, the encoding matrix is composed of Fourier coefficients and it is very well-conditioned with condition number equal to 1. The sensitivity encoding, however, introduces irregularities into the GEM and increases its condition number dramatically. It should be noted that such a large condition number of GEM is not necessarily a serious problem for Cartesian k-space trajectories. This is because for these cases parallel imaging techniques, such as SENSE, can successfully "decouple" the sensitivity encoding from Fourier encoding, and meanwhile divide the sensitivity encoding into small matrices in a pixel-by-pixel fashion. In this way, decoding can be performed by independently inverting such relatively well-conditioned small sensitivity matrices.

In contrast, the whole GEM, containing all the irregular sensitivity encoding, has a condition number much larger than these small sensitivity matrices. As a consequence, the iterative non-Cartesian SENSE reconstruction inevitably encounters the ill-conditioning problem.

Intrinsic Regularization Effect and Semi-Convergence Behavior of the CG Method

Let $E = U\Sigma V^T = \sum_{i=1}^{n} u_i\sigma_i{v_i}^T$ be the singular value decomposition (SVD) of the $m \times n$ GEM E, where $\Sigma = diag(\sigma_1,\sigma_2,\ldots\sigma_n)$ with the numbers $\sigma_1,\sigma_2,\ldots\sigma_n$ denoting the singular values, $U = (u_1,u_2,\ldots,u_n)$ and $V = (v_1,v_2,\ldots,v_n)$ with u_i and v_i are the left and right singular vectors of E, respectively.

The least squares solution for Eq. [2] can then be represented by (12)

$$m_{LS} = \sum_{i=1}^{rank(E)} \frac{{u_i}^T s}{\sigma_i} v_i \quad [4]$$

As we have mentioned above, usually the dimension of GEM is rather large and solving Eq. [3] is unfortunately an ill-posed problem, that is, E has a cluster of small singular values that gradually decay to zero (12); and in Eq. [4] the SVD components corresponding to these small singular values tend to amplify the noise and make the reconstruction unstable. For a discrete ill-posed problem, numerical regularization is a very often used tool to stabilize the solution and optimize SNR. The basic principle of regularization is to "smooth" the solution by truncating or

damping the small singular value components. In this manner, noise amplification can be suppressed.

The CG iteration method, on the other hand, fortunately has an intrinsic regularization effect (12–14). When applied to discrete ill-posed problems, it initially picks up those SVD components corresponding to the largest singular values in Eq. [4], in such a way that the iteration number can be considered as a regularization parameter. In other words, the spectral components of the solution in Eq. [4] associated with the large eigenvalues tend to converge faster than the small ones. As the iteration number increases, more and more small singular values are captured and the degree of regularization decreases. When CG is applied to the normal equation, Eq. [3], the same behavior is observed since the singular values of E^HE are simply the squares of those of E. From this perspective, the CG algorithm has an intrinsic regularization effect when stopped long before the convergence to the least squares solution sets in. Each iteration vector is a regularized solution, and the number of iterations is the regularization parameter. This phenomenon is referred to as semi-convergence because the iteration vector initially approaches the desired exact solution and, then, in later stages of the iterations, converges to some other undesired vector.

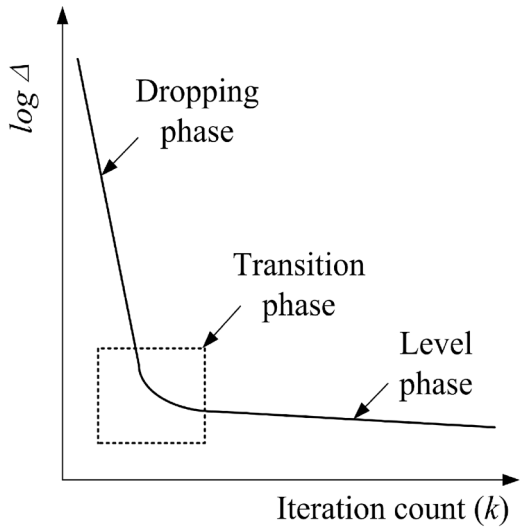

FIG. 1. Plot of residual norm (in *log* scale) versus iteration count for a typical CG iterative reconstruction. The L-curve is divided into 3 segments, which correspond to "dropping phase," "transition phase," and "level phase," respectively.

The Stopping Criterion

The semi-convergence of the CG method raises a very important practical issue in implementation of the iterative non-Cartesian SENSE reconstruction: the stopping rule for iteration. Basically, the iteration should be automatically stopped whenever the iteration vector reaches the best image quality and later iterations will only deteriorate the image. Based on the analysis above, since CG iteration is an intrinsic regularization method and the number of iterations k is the regularization parameter, the stopping criterion is equivalent to the choice of regularization parameter, and thereby it is related to the balance between artifacts and SNR.

CG has a desirable property that if the starting vector is zero, the solution norm increases monotonically with k and, on the other hand, the residual norm decreases monotonically with k (12,14). At a closer look, the residual norm declines very fast at early stages of iteration and then levels off. For a well behaved reconstruction, the plot of the residual norm in *log* scale versus the iteration count usually exhibits an L-curve characteristic, as shown in Fig. 1. In this fashion, the iteration procedure can be divided into 3 phases. At the left of the L-corner, the residual norm declines sharply and it is referred to as a "dropping phase"; at the right side, the residual norm levels off and it is a "level phase." The vicinity of the distinct L-corner then represents the "transition phase," where the artifact and SNR are generally well compromised.

An operational definition of the "corner" is the point on the curve that has maximum curvature (12). Let $m(k)$ denote the kth iteration vector, that is, the intermediate solution for Eq. [3] after k iterations. The residual norm can be represented as

$$\Delta(k) = \|E^HEm(k) - E^Hs\|_2.$$

Let

$$\delta(k) = \log\Delta(k)$$

The curvature is then defined by

$$\kappa(k) = \frac{\delta^n}{((\delta')^2 + 1)^{3/2}} \qquad [5]$$

where differentiation is with respect to the regularization parameter k. Since the residual norm $\Delta(k)$ can be computed as a byproduct in each CG iteration loop, the L-corner can be identified at very modest computational cost.

Generally, the CG iteration should be stopped within the transition phase where artifact and SNR are relatively well compromised and good overall image quality is achieved. However, it is practically difficult to locate the point where artifact and noise are "optimally" compromised and "best" image quality is achieved. In fact, a generally "optimal" stopping rule for the iteration may be nonexistent. First, the best balance between SNR and artifact is highly dependent on specific applications; thus, it is recommended that a relative freedom to choose the iteration number should be provided for customization. Second, since the iterations yield both relatively noise-free and relatively artifact-free images, possibility is provided to pick a number of images in the transition phase for better presentation of the reconstruction results.

In implementation, the iteration is actually not stopped near the L-corner. Note that a number of iterations beyond the stopping criterion are necessary for constructing the L-curve and identifying the corner. Each iteration vector is saved during the iteration process; and once the transition phase is identified, the iteration stops. Finally, the sequence of iteration vectors (images) is retrospected, and

FIG. 2. Sketch of the 8-element head coil for simulations of radial SENSE imaging.

one or several images are selected from the transition phase as the final reconstruction results.

METHODS

The semi-convergence phenomenon of iterative non-Cartesian SENSE reconstruction is demonstrated by both simulations and in vivo experiments. Algorithms were implemented in MATLAB on an IBM PC with Pentium M 1.5G CPU and 512M ram.

Computer Simulation

Sensitivity encoded radial imaging with iterative reconstruction was simulated with different under-sampling rates and varying noise levels. To simulate the parallel MR acquisitions, a typical 8-element head coil array was used whose configuration is sketched in Fig. 2. Sensitivity profiles of these coils were simulated using an analytic integration of the Biot-Savart equation for an axial field of view (FOV). Artificial radial MR data (80 projections $\times$ 256 readout points) were produced from a 256 $\times$ 256 Shepp–Logan phantom image by straightforward Fourier summation (17) along the respective *k*-space trajectories. White noise with varying amplitude was added to the artificial data, with equal variance in all channels. Noise correlation was neglected for simplicity. For reconstruction, in the iteration loops the LS-nuFFT gridding principle was implemented with over-sampling rate 2 and convolution kernel window width 4. A rough time estimate showed that each iteration for a 256 $\times$ 256 reconstruction takes around 4 seconds in our simulations. Both density correction and intensity correction were used for pre-conditioning. The CG algorithm was implemented according to Ref. (11).

In Vivo Experiments

In vivo MRI experiments were performed on a healthy volunteer on a Siemens 3T Trio scanner equipped with 8 independent receiver channels. An 8-element head coil array was employed whose configuration is similar to Fig. 2. Axial brain images were acquired with a 2D spiral sequence (FOV = 200 $\times$ 200 mm, slice thickness = 3 mm, TR = 3s, flip angle = 80°). In this experiment, a full dataset with 4 interleaves for 128 $\times$ 128 imaging was acquired. In the readout direction, 3908 samples were acquired for each interleaf with standard sampling density. The full dataset was later decimated off-line by extracting 1 or 2 interleaves for reconstruction, corresponding to acceleration factors 2 and 4, respectively. Coil sensitivities were calculated using the method described in Ref. (7) from the full dataset. The same gridding method and CG algorithm as in simulations were implemented for reconstruction.

RESULTS

Computer Simulations

The results of computer simulations are summarized in Fig. 3. The intermediate images after 1, 3, 5, 15, and 30 iterations with different sampling schemes and noise levels are presented. Specifically, Figs. 3a, 3b, and 3c show the reconstruction from 40, 80, and 20 projections, respectively, with matrix size 256 $\times$ 256 and noise level -17dB with respect to the average signal intensity. Fig. 3d shows the images reconstructed from 40 projections with noise level -10dB. For each image sequence, it is obvious that the overall image quality exhibits a typical convergence-divergence behavior, that is, it at first improves with the number of iterations, and in later stages begins to deteriorate. In particular, as predicted in the Theory section, the aliasing artifacts decrease monotonically with the iteration number, while the noise level increases. At early stages, the images are dominated by streaking artifacts typical for radial undersampling; while at late stages, they are dominated by noise. There is a transition phase where the artifact and noise level are well compromised and relatively high image quality is achieved.

It has been demonstrated in Ref. (11) that the convergence behavior is strongly dependent on the degree of reduction *R*. When *R* increases, the condition of the underlying GEM deteriorates and consequently the convergence slows down. In our simulations, the same phenomenon is observed by comparing Figs. 3a, 3b, and 3c. For the reconstruction with fewer projections, higher artifact and lower SNR are achieved at all the iteration counts and the convergence is slower. As a supplement to Pruessmann's description, it is found that in the later divergence phase, the divergence trend is faster, that is, the image deteriorates faster for a higher undersampling rate. This is because for a higher acceleration rate, the reconstruction is worse ill-conditioned and more sensitive to the regularization parameter.

The influence of noise level on CG iterative reconstruction can be revealed by comparing Fig. 3a with Fig. 3d. At the first several stages, although the noise levels in the MR data are quite different for these two reconstructions, the resulting image quality is comparable. However, in late stages of iteration, the image quality with higher noise level deteriorates much faster than that with lower noise level. This phenomenon is due to the intrinsic regularization effect of CG iteration. At the first stages, more regu-

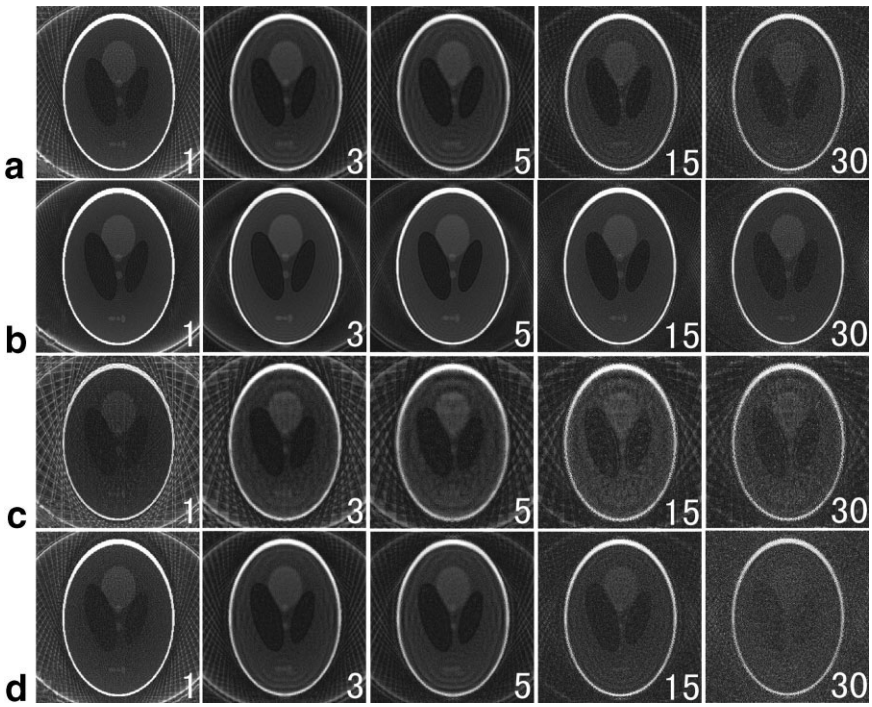

FIG. 3. Simulated iterative reconstructions for sensitivity-encoded radial imaging with: (**a**) 40 projections, (**b**) 80 projections, (**c**) 20 projections, (**d**) 40 projections. For (a–c) the noise level is −17dB with respective to average signal intensity, while for (d) it is −10dB. The number at the lower right corner of each image indicates the iteration count.

larization is applied in the reconstruction, and thereby it is less sensitive to noise. At late stages, less regularization is applied and the noise amplification effect is much more apparent.

In Vivo Experiments

Reconstruction results from the in vivo MRI data are displayed in Figs. 4 and 5. For Fig. 4a, 2 interleaves are extracted from the full dataset for reduction factor 2, and iterative SENSE reconstruction was performed using this undersampled dataset. For Fig. 4b only 1 interleaf was used to simulate fourfold acceleration. Images after 1, 5, 15, 50, and 99 iterations are presented, respectively. Similar with the simulation results, an apparent semi-convergence behavior is observed. With higher acceleration rate, the reconstruction converges slower and diverges faster, as demonstrated by comparing Figs. 4a and 4b, where around 15 iterations is needed for a good reconstruction for twofold reduction (Fig. 4a) and 50 iterations for fourfold reduction (Fig. 4b).

Figs. 5a and 5b show the residual norm (in *log* scale) varying with iteration count for the two reconstructions corresponding to Figs. 4a and 4b, respectively. Both curves exhibit L-shapes, agreeing with our description in the Theory section. For the reconstruction with reduction factor 2, the L-shape is more typical with a more distinct partition of dropping phase and level phase. The L-corners of these two curves correspond to 21 iterations and 55 iterations, respectively, which are marked by triangles on the curves. By comparison of Fig. 4 to Fig. 5, it is easy to see that the intermediate images within the transition phase, for instance, the image after 15 iterations in Fig. 4a and the one after 50 iteration in Fig. 4b, exhibit good compromises between SNR and artifacts and they show the best overall image quality in their respective image sequences.

DISCUSSION

Since the semi-convergence behavior can be accounted for by the ill-conditioning of the reconstruction and the

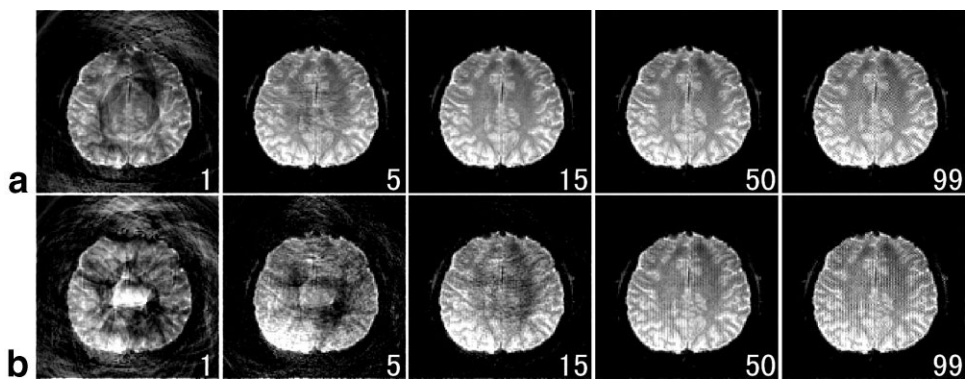

FIG. 4. Sensitivity-encoded brain imaging using an 8-element head coil and 2D spiral acquisition: (**a**) Reduction factor = 2; (**b**) Reduction factor = 4. The number at the lower right corner of each image indicates the iteration count.

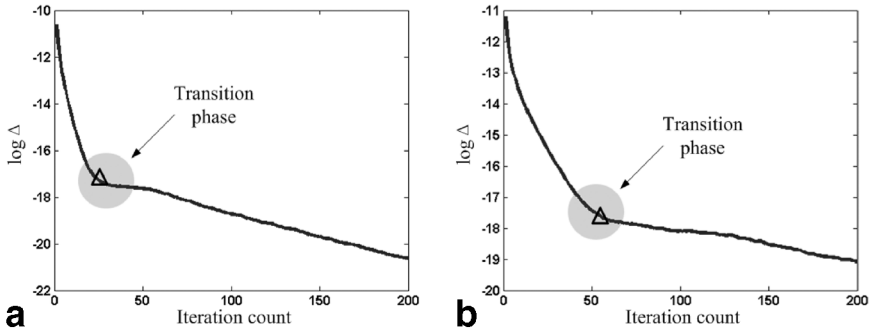

FIG. 5. Plot of residual norm (in *log* scale) versus iteration count for the reconstructions of in vivo spiral imaging corresponding to Fig. 4: (**a**) Reduction factor = 2; (**b**) Reduction factor = 4. The L-corners are indicated by triangles and the transition phases are indicated by gray circles. It is shown that the best images in Figs. 4a and 4b are both within the transition phases of the reconstructions.

regularizing nature of CG iteration, it is conceivable that the convergence behavior of reconstruction is affected by both encoding-related factors and reconstruction-related factors. The encoding-related factors, such as the acquisition trajectory, the reduction factor, the noise level in samples, and the coil array geometry employed for acquisition, determine the condition of the reconstruction and thereby affect its convergence behavior. The reconstruction-related factors, on the other hand, affect the implementation of the CG iteration. For example, it has been demonstrated in Eggers's works that the regridding method employed (18), the preconditioner used (11,19), and the initialization of iteration (20) all affect the convergence behavior.

Besides a suitable well-defined stopping criterion, a second option to cope with the semi-convergence behavior is to apply explicit Tikhonov regularization to Eq. [3] (19). By improving the numerical condition of the large GEM, the semi-convergence of the reconstruction can be overcome. One difficulty of this strategy is how to optimize the regularization parameter. Further investigation on this issue would be interesting.

CONCLUSIONS

The convergence behavior of iterative non-Cartesian SENSE reconstruction has been investigated in this work. It has been revealed that the semi-convergence behavior is caused by the ill-conditioning of reconstruction and the intrinsic regularization effect of CG iteration. Simulations and MR experiments have shown that the convergence behavior of iterative non-Cartesian SENSE reconstruction is highly related to SNR and level of artifacts. There is a transition phase during the iteration process where the SNR and artifacts are relatively well compromised and satisfactory overall image quality can be achieved. Suggestions with respect to the stopping criterion have also been provided.

ACKNOWLEDGMENTS

The authors thank Dr. Hua Guo for helpful discussion and Dr. Gunnar Krueger of Siemens Medical Solutions for providing the spiral fMRI sequence.

REFERENCES

1. Hutchinson M, Raff U. Fast MRI data acquisition using multiple detectors. Magn Reson Med 1998;6:87–91.
2. Sodickson DK, Manning WJ. Simultaneous acquisition of spatial harmonics (SMASH): fast imaging with radiofrequency coil arrays. Magn Reson Med 1997;38:591–603.
3. Sodickson DK. Tailored SMASH image reconstructions for robust in vivo parallel MR imaging. Magn Reson Med 2000;44:243–251.
4. Bydder M, Larkman DJ, Hajnal JV. Generalized SMASH imaging. Magn Reson Med 2002;47:160–170.
5. Heidemann RM, Griswold MA, Haase A, Jakob PM. VD-AUTO-SMASH imaging. Magn Reson Med 2001;45:1066–1074.
6. Griswold MA, Jakob PM, Heidemann RM, Nittka M, Jellus V, Wang J, Kiefer B, Haase A. Generalized Auto-Calibrating Partially Parallel Acquisition (GRAPPA). Magn Reson Med 2002;47:1202–1210.
7. Pruessmann KP, Weiger M, Scheidegger MB, Boesiger P. SENSE: sensitivity encoding for fast MRI. Magn Reson Med 1999;42:952–962.
8. Sodickson DK, McKenzie CA. A generalized approach to parallel magnetic resonance imaging. Med Phys 2001;28:1629–1643.
9. Pruessmann KP, Weiger M, Bornert P, Boesiger P. A gridding approach for sensitivity encoding with arbitrary trajectories. In: Proc ISMRM 8th Annual Meeting, Denver, 2000. p 276.
10. Kannengießer SAR, Brenner AR, Noll TG. Accelerated image reconstruction for sensitivity encoded imaging with arbitrary k-space trajectories. In: Proc ISMRM 8th Annual Meeting, Denver, 2000. p 155.
11. Pruessmann KP, Weiger M, Bornert P, Boesiger P. Advances in sensitivity encoding with arbitrary k-space trajectories. Magn Reson Med 2001;46:638–651.
12. Hansen PC. Rank-deficient and discrete ill-posed problems: numerical aspects of linear inversion. Philadelphia: SIAM; 1998.
13. Hanke M. Conjugate gradient type methods for ill-posed problems. Pitman Research Notes in Mathematics Series, 327: Harlow, UK; Longman Scientific & Technical; 1995.
14. Van der Sluis A, Van der Vorst HA. The rate of convergence of conjugate gradients. Numer Math 1986;48:543–560.
15. Sha L, Guo H, Song AW. An improved gridding method for spiral MRI using nonuniform fast Fourier transform. J Magn Reson. 2003;162:250–258.
16. Zhang B, Zhong K, Wang J, Zhuo Y. LS-nuFFT based SENSE reconstruction for polar k-space trajectory. In: Proc ISMRM 12th Annual Meeting, Kyoto, 2004. p 450.
17. Sarty GE. The natural k-plane coordinate reconstruction method for magnetic resonance imaging: mathematical foundations. Int J Imaging Syst Technol 1997;8:519–528.
18. Eggers H, Bornert P, Boesiger P. Comparison of gridding- and convolution-based iterative reconstruction algorithms for sensitivity-encoded non-Cartesian acquisition. In: Proc ISMRM 10th Annual Meeting, Honolulu, 2002. p 130.
19. Eggers H, Boesiger P. Improved preconditioning for the non-Cartesian SENSE reconstruction with regularization. In: Proc ISMRM 12th Annual Meeting, Kyoto, 2004. p 449.
20. Eggers H, Bornert P, Boesiger P. Improved initialization of the iterative reconstruction for sensitivity-encoded non-Cartesian imaging. In: Proc ISMRM 11th Annual Meeting, Toronto, 2003. p 5.